

Journal: Monthly Notices of the Royal Astronomical Society
Article doi: 10.1093/mnras/stv1081
Article title: Results of two multichord stellar occultations by dwarf planet (1) Ceres
First Author: A. R. Gomes-Júnior
Corr. Author: J. I. B. Camargo



INSTRUCTIONS

We encourage you to use Adobe's editing tools (please see the next page for instructions). If this is not possible, please list clearly in an e-mail. Please do not send corrections as track changed Word documents.











Changes should be corrections of typographical errors only. Changes that contradict journal style will not be made.

These proofs are for checking purposes only. They should not be considered as final publication format. The proof must not be used for any other purpose. In particular we request that you: do not post them on your personal/institutional web site, and do not print and distribute multiple copies. Neither excerpts nor all of the article should be included in other publications written or edited by yourself until the final version has been published and the full citation details are available. You will be sent these when the article is published.

1. **Licence to Publish:** Oxford Journals requires your agreement before publishing your article. If you haven't already completed this, please sign in with your My Account information and complete the online licence form. Details on how to do this can be found in the Welcome to Oxford Journals email.
 2. **Permissions: Permission to reproduce any third party material in your paper should have been obtained prior to acceptance. If your paper contains figures or text that require permission to reproduce, please inform me immediately by email.**
 3. **Author groups:** Please check that all names have been spelled correctly and appear in the correct order. Please also check that all initials are present. Please check that the author surnames (family name) have been correctly identified by a pink background. If this is incorrect, please identify the full surname of the relevant authors. Occasionally, the distinction between surnames and forenames can be ambiguous, and this is to ensure that the authors' full surnames and forenames are tagged correctly, for accurate indexing online.
 4. **Figures:** If applicable, figures have been placed as close as possible to their first citation. Please check that they are complete and that the correct figure legend is present. Figures in the proof are low resolution versions that will be replaced with high resolution versions when the journal is printed.
 5. **Missing elements:** Please check that the text is complete and that all figures, tables and their legends are included.
 6. **Special characters and equations:** Please check that special characters, equations and units have been reproduced accurately.
 7. **URLs:** Please check that all web addresses cited in the text, footnotes and reference list are up-to-date.
 8. **Funding:** If applicable, any funding used while completing this work should be highlighted in the Acknowledgements section. Please ensure that you use the full official name of the funding body.
-

AUTHOR QUERIES - TO BE ANSWERED BY THE CORRESPONDING AUTHOR

The following queries have arisen during the typesetting of your manuscript. Please answer these queries by marking the required corrections at the appropriate point in the text.

Query No.	Nature of Query	Author's Response
Q1	Author: The figures have been processed according to information entered by you during the submission of your manuscript. Please note that if you have confirmed that you wish to publish your figures in colour in print and that you are willing to pay the £200 (+VAT) charge, you will be invoiced upon publication. Black and white versions of figures are provided at the end of the paper. Please check the black and white versions to assess their quality for the print version of the journal, and contact us if you have any concerns.	
Q2	Author: Please supply email addresses for between one and three authors who are willing to correspond with readers and for their email address to be included in the article	
Q3	Author: To check that we have your surnames correctly identified and tagged (e.g. for indexing), we have coloured pink the names that we have assumed are surnames. If any of these are wrong, please let us know so that we can amend the tagging.	
Q4	Author: Most of the affiliations do not have postal codes. Please provide the postal codes, if required.	
Q5	Author: If you refer to any data bases in your paper, please note the journal policy for properly crediting those responsible for compiling the data base. Rather than citing only a URL, if at all possible please also cite a reference (and include it in the reference list), or if a reference is not available then the names of those who compiled the data base. Note that some data bases do provide guidelines on how they should be cited – please check for these and follow them in your paper where appropriate.	
Q6	Author: The MNRAS list of approved key words has been revised and updated. The new list is appended to these proofs. If you had previously selected key words from the old list, please now check them carefully against the new list in case they need to be changed, or there are new ones that you would like to add. If you had not previously selected key words from the MNRAS approved list, please now choose up to six from the new list.	
Q7	Author: Please check the figures in the PDF proof carefully.	
Q8	Author: Please note that computer software/programming languages must be styled in SMALL CAPITAL LETTERS, according to journal style. Please check and correct this paper accordingly.	
Q9	Author: Please check whether the reference is okay as amended.	
Q10	Author: Please update this reference, if possible, with full details to be added to the references list (all authors must be listed if there are eight or fewer).	



MAKING CORRECTIONS TO YOUR PROOF

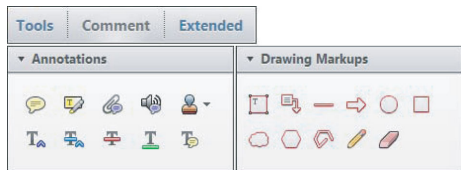
These instructions show you how to mark changes or add notes to the document using the Adobe Acrobat Professional version 7 (or onwards) or Adobe Reader X (or onwards). To check what version you are using go to **Help** then **About**. The latest version of Adobe Reader is available for free from get.adobe.com/reader.

Displaying the toolbars

Adobe Professional X, XI and Reader X, XI

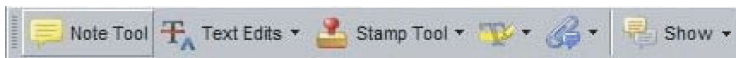
Select **Comment, Annotations and Drawing Markups**.

If this option is not available, please let me know so that I can enable it for you.



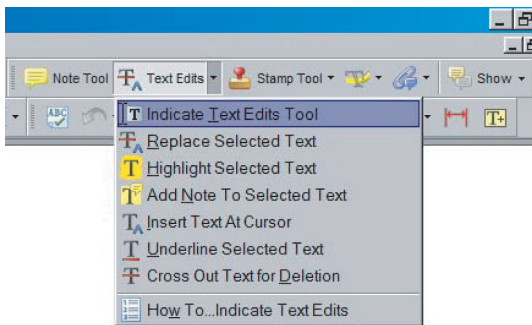
Acrobat Professional 7, 8 and 9

Select **Tools, Commenting, Show Commenting Toolbar**.



Using Text Edits

This is the quickest, simplest and easiest method both to make corrections, and for your corrections to be transferred and checked.



1. Click **Text Edits**
2. Select the text to be annotated or place your cursor at the insertion point.
3. Click the **Text Edits** drop down arrow and select the required action.

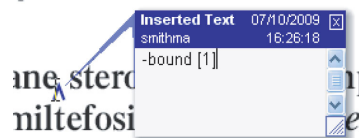
You can also right click on selected text for a range of commenting options.

SAVING COMMENTS

In order to save your comments and notes, you need to save the file (**File, Save**) when you close the document. A full list of the comments and edits you have made can be viewed by clicking on the Comments tab in the bottom-left-hand corner of the PDF.

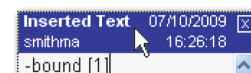
Pop up Notes

With *Text Edits* and other markup, it is possible to add notes. In some cases (e.g. inserting or replacing text), a pop-up note is displayed automatically.



To **display** the pop-up note for other markup, right click on the annotation on the document and selecting **Open Pop-Up Note**.

To **move** a note, click and drag on the title area.



To **resize** of the note, click and drag on the bottom right corner.



To **close** the note, click on the cross in the top right hand corner.



To **delete** an edit, right click on it and select **Delete**. The edit and associated note will be removed.

Q1 Results of two multichord stellar occultations by dwarf planet (1) Ceres

5 A. R. Gomes-Júnior,^{1★} B. L. Giacchini,^{2,3,4} F. Braga-Ribas,^{5,6†} M. Assafin,^{1††} 67
 R. Vieira-Martins,^{1,5††} J. I. B. Camargo,^{5†} B. Sicardy,⁷ B. Timerson,⁴ T. George,⁴
 J. Broughton,⁸ T. Blank,⁴ G. Benedetti-Rossi,⁵ J. Brooks,⁴ R. F. Dantowitz,⁹
 10 D. W. Dunham,⁴ J. B. Dunham,⁴ C. K. Ellington,⁴ M. Emilio,¹⁰ F. R. Herpich,¹¹ 72
 Q2 C. Jacques,^{3,12} P. D. Maley,^{4,13} L. Mehret,¹⁰ A. J. T. Mello,¹⁴ A. C. Milone,¹⁵
 Q3 E. Pimentel,^{3,12} W. Schoenell¹¹ and N. S. Weber⁹

¹Observatório do Valongo/UFRJ, Ladeira Pedro Antônio 43, CEP 20.080-090 Rio de Janeiro – RJ, Brazil

²Centro Brasileiro de Pesquisas Físicas, Rua Dr Xavier Sigaud 150, Rio de Janeiro 22290-180, Brazil

Q4 ³Seção de Ocultações/REA-Brasil, Belo Horizonte, Brazil

⁴International Occultation Timing Association, PO Box 131034, Houston, TX 77219-1034, USA

⁵Observatório Nacional/MCTI, R. General José Cristino 77, CEP 20921-400 Rio de Janeiro – RJ, Brazil

⁶Federal University of Technology – Paraná (UTFPR / DAFIS), Rua Sete de Setembro, 3165, CEP 80230-901, Curitiba, PR, Brazil

20 ⁷LESIA, Observatoire de Paris, CNRS UMR 8109, Université Pierre et Marie Curie, Université Paris-Diderot, 5 place Jules Janssen,
 F-92195 Meudon Cedex, France 82

⁸RASNZ Occultation Section, PO Box 3181, Wellington, New Zealand

⁹Clay Center Observatory at Dexter Southfield, 20 Newton Street, Brookline, MA 02445, USA

¹⁰Universidade Estadual de Ponta Grossa, Ponta Grossa, Brazil

25 ¹¹Universidade Federal de Santa Catarina, Florianópolis, Brazil

¹²Centro de Estudos Astronômicos de Minas Gerais, Belo Horizonte, Brazil

¹³NASA Johnson Space Center Astronomical Society, Houston, TX, USA

¹⁴Federal University of Technology – Paraná (UTFPR / DAELT), Rua Sete de Setembro, 3165, CEP 80230-901, Curitiba, PR, Brazil

¹⁵Instituto Nacional de Pesquisas Espaciais, São José dos Campos, Brazil

30 Accepted 2015 May 11. Received 2015 May 9; in original form 2015 April 11

ABSTRACT

35 Q5 We report the results of two multichord stellar occultations by the dwarf planet (1) Ceres that 97
 were observed from Brazil on 2010 August 17, and from the USA on 2013 October 25. Four
 positive detections were obtained for the 2010 occultation, and nine for the 2013 occultation.
 40 Elliptical models were adjusted to the observed chords to obtain Ceres' size and shape. Two 102
 limb-fitting solutions were studied for each event. The first one is a nominal solution with
 an indeterminate polar aspect angle. The second one was constrained by the pole coordinates
 as given by Drummond et al. Assuming a Maclaurin spheroid, we determine an equatorial
 45 diameter of 972 ± 6 km and an apparent oblateness of 0.08 ± 0.03 as our best solution. These 107
 results are compared to all available size and shape determinations for Ceres made so far, and
 shall be confirmed by the NASA's *Dawn* space mission.

Key words: occultations – minor planets, asteroids: individual (1, Ceres) – planets and satel-
 Q6 lites: fundamental parameters. 112

1 INTRODUCTION

55 Ceres is the sole example of a dwarf planet in the inner Solar sys-
 tem. Far from being mere taxonomic information, this suggests

*E-mail: altair08@astro.ufrj.br

†Associated to Laboratório Interinstitucional de e-Astronomia - LIneA, Rua
 60 Gal. José Cristino 77, CEP 20921-400, Rio de Janeiro, Brazil.

††Affiliated researcher at Observatoire de Paris/IMCCE, 77 Avenue Denfert
 Rochereau, F-75014 Paris, France.

the great impact its study can have on the understanding of plan-
 etary formation and evolution of the Solar system. Indeed, it was
 proposed that Ceres' origin could have been as a trans-Neptunian
 object (McKinnon 2012), later scattered to the Main Belt due to
 the giant planets' migration predicted by the 'Nice Model' (Gomes
 et al. 2005). Even if it was formed close to its current location, the
 dynamical history of the Solar system must have left its signatures
 on Ceres. These could include not only the late heavy bombard-
 ment features that might exist on its surface, but also the makeup
 of its volatiles, which could have been transported from the outer
 region.

Table 1. Circumstances of observation for all observing stations of the 2010 event.

Site	Longitude Latitude Height	Telescope Aperture f-ratio	Exposure Cycle time Camera	Result Ingress Egress	Observer
Belo Horizonte CEAMIG-REA	43°59'51" W 19°49'49" S 825 m	LX200 31 cm f/10	5 s 12 s SBIG ST10	Positive 22:39:03.9 ± 0.6 s 22:40:20 ± 5 s	C. Jacques E. Pimentel
Pico dos Dias LNA	45°34'45" W 22°32'03" S 1864 m	Zeiss 60 cm f/12.5	1 s 2 s Andor Ikon	Positive 22:37:30.3 ± 0.6 s 22:41:55.3 ± 0.7 s	J. I. B. Camargo G. B. Rossi
São José dos Campos INPE	45°51'44" W 23°12'33" S 620 m	C11 28 cm f/6.3	2 s 5 s SBIG ST7	Egress only Start obs.: 22:39:44 22:42:03.0 ± 0.2 s	A. C. Milone T. Maldonado M. Okada
Ponta Grossa UEPG	50°05'56" W 25°05'22" S 910 m	RCX 400 40 cm f/8	30 s 52 s SBIG STL6E	Positive 22:37:17 ± 13 s 22:39:56 ± 13 s	M. Emilio L. Mehret
Florianópolis UFSC	48°31'20" W 27°36'12" S 20 m	C11 28 cm f/10	3 s 6 s SBIG ST7	No occultation Start obs.: 21:49:27 End obs.: 22:51:21	W. Schoenell A. J. T. Mello F. R. Herpich

Since the 1970s it has been speculated that Ceres could contain water ice, which was recently verified (Küppers et al. 2014). Although the water regime on this object is still unknown, some internal structure models suggest the existence of a water vapour – or even a liquid water – layer (Castillo-Rogez 2011). Yet the very question of whether Ceres underwent differentiation is open and, on the assumption of an affirmative answer, it is natural to ask if it ever had tectonics, what its geological evolution was, and if it is still active. Inarguably NASA's *Dawn* mission (Russell et al. 2004), which is currently orbiting the dwarf planet, will shed light on several open issues concerning Ceres.

Containing approximately one-fifth of the whole Main Belt's mass, Ceres is expected to have an equilibrium figure, i.e. a Maclaurin or a Jacobi ellipsoid. In fact, direct observations of Ceres by means of adaptive optics indicate that it is an oblate spheroid (Drummond et al. 2014). The precise knowledge of its size and shape is of utmost importance, for the models of density, internal structure, and differentiation.

The best ground-based technique for determining shape and size of a faraway object is the study of its shadow, cast by a star during an occultation. Since the 1960s occultations have provided measurements of hundreds of asteroids, thanks partially to the fruitful professional–amateur collaboration on the field. More recently, this technique has been applied to objects of the outer Solar system and has unveiled outstanding features of distant bodies, e.g. the ring system around the Centaur (10199) Chariklo (Braga-Ribas et al. 2014).

The first stellar occultation by Ceres was observed in 1984 (Millis et al. 1987) and led to the determination of its size to the precision of some kilometres, at a time when the uncertainties were often ten times larger. The high apparent brightness of Ceres, as compared to most asteroids, imposes a somewhat strong constraint on the stars capable of causing a detectable magnitude drop when occulted. For instance, after the 1984 event, to our knowledge, only four stellar occultations have been observed (Dunham et al. 2014). Two of them had only two chords each, thus not sufficient for providing accurate results.¹ The two remaining events, which occurred on 2010 August 17 and 2013 October 25, are reported in the present work and are

the first ones that used charged-couple devices (CCD) as recording systems. Throughout the paper we shall refer to these events as the '2010 occultation' and the '2013 occultation'.

Both events were predicted by Steve Preston² on behalf of the International Occultation Timing Association, during routine prediction of asteroidal occultations of bright stars.

This work is organized as follows. In Sections 2 and 3 we analyse the 2010 and the 2013 occultations, respectively. In Section 4 we give the geocentric positions of Ceres derived from the occultations. The comparison of our results to those in the literature is carried out in Section 5.

2 THE 2010 OCCULTATION

2.1 Observations

As predicted, on 2010 August 17 Ceres occulted the star TYC 6833-163-1 (UCAC4 313-111823), which has magnitude $V = 11.55$ and has the ICRS position, based on UCAC4 catalogue (Zacharias et al. 2013), to the date of occultation:

$$\begin{cases} \alpha = 17^{\text{h}}18^{\text{m}}29^{\text{s}}.0085 \\ \delta = -27^{\circ}26'38''.867. \end{cases} \quad (1)$$

Observations were carried out in Brazil from five different sites as displayed in Table 1 and Fig. 1. The occultation was detected from four of them. The southernmost one (UFSC) had a negative chord. From the positive sites, the one named INPE started observing after the event was already in progress, due to technical difficulties, thus providing only the star's reappearance time; the other three recorded the whole phenomenon.

A remarkable circumstance of this event was the low velocity of Ceres: only 3.9 km s^{-1} in the plane of the sky. Therefore, even exposures of a few seconds would translate in a relevant spatial resolution.

All the observations were made through a sequence of images obtained with CCDs. The times of each exposure were available on the header of each image with an internal accuracy of a few

¹ These events took place on 1994 August 22 and 2010 October 30.

² Predictions are published at <http://asteroidoccultation.com>

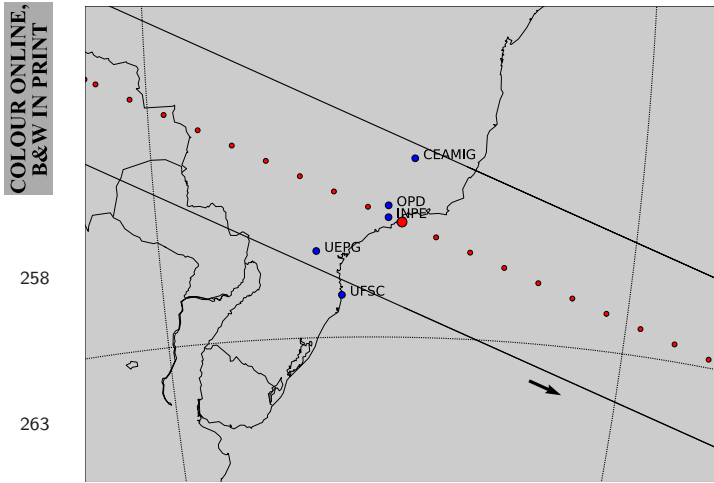


Figure 1. Post-occultation reconstruction of Ceres' shadow path on Earth for the 2010 August 17 event. The big red dot is the geocentric closest approach at 22:40:25 UT. The small red ones represent the centre of the shadow separated by one minute, shadow moves from the left to the right. Blue dots are the sites that have observed the event. As described in text, UFSC had a negative chord.

hundredths of a second. CEAMIG had only the integer part of the second available, due to the acquisition software used. The fraction of a second could be retrieved as described on the section 3.1 of Braga-Ribas et al. (2013, which shall be referred as BR13 hereafter). Cycle times (exposure plus read-out) varied from 2 to 52 s, as can be verified in Table 1, making it a heterogeneous set of observations and imposing an error of a few seconds for the ingress/egress times of some sites.

2.2 Light curves

The flux of the star in the five occultation chords was obtained from the FITS images with the Platform for Reduction of Astronomical Images Automatically (PRAIA) (Assafin et al. 2011). The light curves were normalized to the flux of the star plus Ceres, as they were merged right before and after the occultation. Additionally, they were normalized by fitting a polynomial curve (of first or second order) outside the flux drop, so that the flux ratio was set to 1 outside the occultation.

The ingress (disappearance) and egress (reappearance) instants of the occultation were obtained for each light curve by fitting a square-well model convoluted with the Fresnel diffraction, the CCD bandwidth, the stellar apparent diameter, and the applied finite exposure time; see Widemann et al. (2009) and BR13. The smallest integration time used in the positive observations was 1.0 s, which translates to almost 3.9 km in the celestial plane. Therefore, the error on the time determination of the ingress and egress is largely dominated by the integration times, not by Fresnel diffraction or star diameter, which are both of the order of a few hundred metres for this event. The occultation data fit consists in minimizing a classical χ^2 function for each light curve, as described in Sicardy et al. (2011) and BR13. The free parameter to adjust is the ingress or egress instant, which provides the minimum value of χ^2 , denoted as χ^2_{\min} . The best fittings to the 2010 occultation light curves are shown in Fig. 2, and the derived occultation times are listed in Table 1.

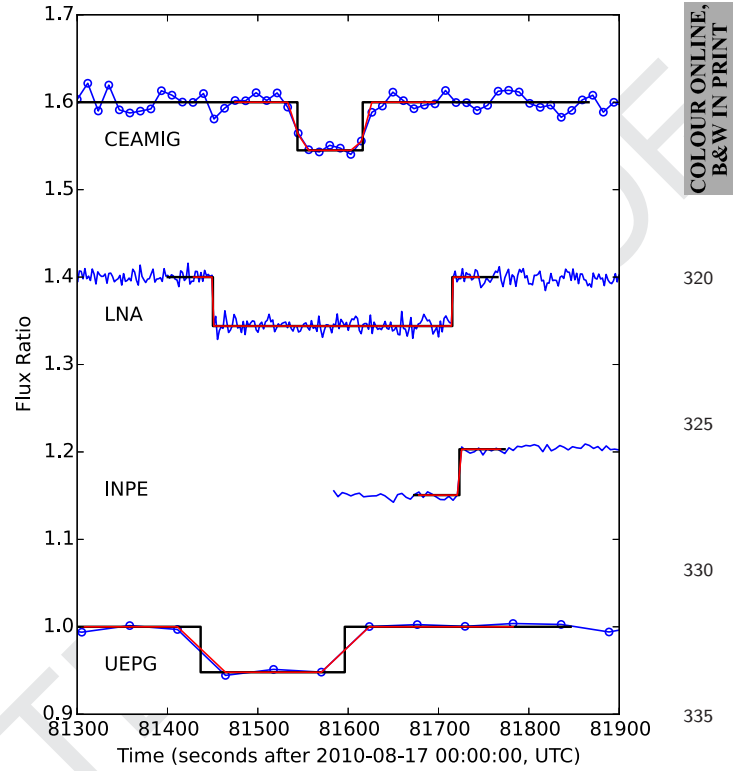


Figure 2. The four occultation light curves normalized and vertically shifted by a factor of 0.2 for better visualization. The solid black lines are the best fit of the square-well model to the data. Red lines are the square-well model convoluted with the Fresnel diffraction, the star diameter, and the applied exposure time. The mid-times of the occultations do not coincide due to the propagation delays of the shadow due to the distinct longitude of the sites. Exposures at INPE started after the immersion, as explained in the text.

2.3 Limb-fitting methodology

The methodology used to analyse Ceres' profile from the observations is the same described by Sicardy et al. (2011) and BR13. Each combination of site position and recorded ingress/egress instant, together with star coordinates and Ceres' ephemeris, corresponds to a point in the plane of the sky. The collection of all these points ideally determines the apparent limb of Ceres.

We adopt an elliptic model for the limb profile, resulting from the projection of an oblate spheroid on to the sky plane. This choice is supported by the work of Drummond et al. (2014), by means of direct imaging of Ceres. Hence, we have $N = 7$ chord extremities to adjust the $M = 5$ parameters which define an ellipse: apparent semimajor and semiminor axis (a' and b' , respectively), position angle P of its semiminor axis and the position (f_c , g_c) of its centre with respect to the occulted star. Of course, the apparent semimajor axis a' is equivalent to the equatorial radius R_{equa} of the ellipsoid. The coordinates f_c and g_c , in kilometres, are calculated using the JPL#33 Ceres' ephemeris (Giorgini et al. 1996) and the occulted star's position. They are positive towards the local celestial east and north, respectively. The position angle P is counted positively from the direction of local celestial north to celestial east. The apparent oblateness can be defined by $\epsilon' = 1 - (b'/a')$. The best-fitting solution is obtained minimizing a reduced χ^2_r function, where we define the number of degrees of freedom of the problem as $\mathcal{N} \equiv N - M$. All the procedures that allow the determination of the error bars of the physical parameters can be found in BR13.

Table 2. Results of limb fitting to the data of the 2010 and 2013 events.

Solution	2010/Nominal	2010/Pole-constrained	2013/Nominal	2013/Pole-constrained
Equatorial diameter (km)	982 ± 14	972 ± 6	971 ± 7	971 ± 7
True oblateness	0.08 ± 0.03	0.08 ± 0.03	0.08 ± 0.04	0.08 ± 0.04
Position angle (deg)	5 ± 10	12 ± 3 (*)	22 ± 5	25 ± 3 (*)
f_c (km)	97 ± 9	102 ± 5	77 ± 6	78 ± 6
g_c (km)	16 ± 15	21 ± 11	13 ± 16	13 ± 16
$\chi^2_{r,\min}$	0.24	0.42	1.27	1.27

Notes. In bold we highlight our best solution. Error bars are at 1σ level. The polar diameter (D_{pol}) can be easily calculated from $D_{\text{pol}} = D_{\text{equa}}(1 - \epsilon)$. (*) Position angle derived from Ceres' rotational pole coordinates determined by Drummond et al. (2014).

2.4 Limb-fitting solutions

Two possible solutions were considered for the limb fitting. The first, which we call nominal solution, consists of determining the five parameters that characterize an ellipse from the seven observed contacts. As we shortly show, it led to a rather large uncertainty on the position angle. Furthermore, the nominal solution alone is not capable of returning the true oblateness, which can be evaluated through equation 2 of BR13 provided that the aspect angle ζ is known.

It is possible to derive the pole position (ζ, P) from the coordinates of Ceres' pole (α_p, δ_p) and its ephemeris (α, δ) via

$$\begin{cases} \cos(\zeta) = -\sin(\delta_p)\sin(\delta) - \cos(\delta_p)\cos(\delta)\cos(\alpha_p - \alpha) \\ \tan(P) = \frac{\sin(\alpha_p - \alpha)}{\tan(\delta_p)\cos(\delta) - \sin(\delta)\cos(\alpha_p - \alpha)} \end{cases} \quad (2)$$

where $\zeta = 0^\circ$ and $\zeta = 90^\circ$, respectively, correspond to a pole-on and an equator-on geometry.

From observations with adaptive optics spanning a 10-year period, Drummond et al. (2014) determined the position of Ceres' polar axis within an error of only 3° :

$$\alpha_p = (287 \pm 3)^\circ, \quad \delta_p = (+64 \pm 3)^\circ, \quad (3)$$

in equatorial J2000 coordinates. Together with Ceres' ephemeris at the moment of the occultation, this corresponds to the polar aspect angle $\zeta = 86.1^\circ$, which is very close to an equator-on geometry. Hence, we expect true figures to be similar to apparent ones.

The knowledge of Ceres' pole not only allows the determination of its polar aspect, it suffices to set its position angle. Therefore equations (2) and (3) may act as a constraint for P , and a second solution can be obtained by probing the parameter space with the restriction that the position angle is confined to the range that follows from equation (3). We call this the 'pole-constrained solution'.

2.4.1 Nominal solution

With the seven observed contacts it is possible to adjust the five parameters which define an ellipse. For the best-fitting solution we find $\chi^2_{r,\min} = 0.24$, which could be interpreted as a slightly overestimation of the error bars with regard to the good quality of the fit. However, inasmuch as the problem has only two degrees of freedom, it is far from the statistical realm and relatively small $\chi^2_{r,\min}$ are acceptable.

The resulting values of equatorial diameter, oblateness, position angle, and centre coordinates are presented in the second column of Table 2.

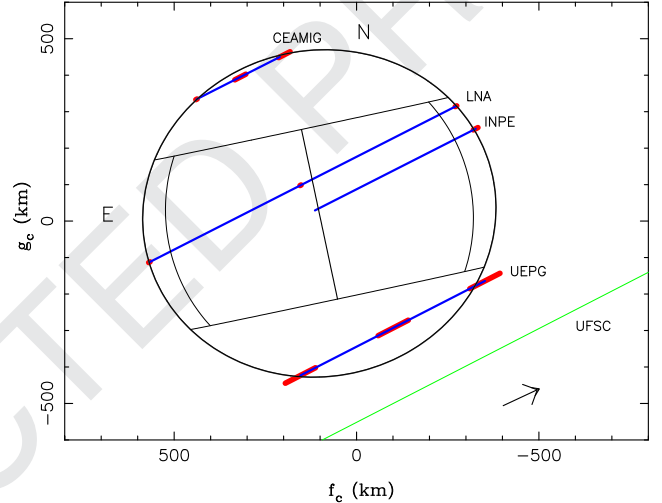


Figure 3. The best elliptical fit for the occultation chords for the event of 2010 using the times from Table 1 and the pole-constrained solution. The arrow indicates the direction of motion, blue lines are the observed chords, the red segments are the ingress, egress and mid-occultation error bars at 1σ level.

Already mentioned, the parameter with the largest uncertainty is the position angle: spanning on a 20° interval, its determination has a relative precision worse than 10 per cent. Clearly, the coordinates of Ceres' pole (equation 3) can impose a strong constraint on the position angle, as the next solution shows.

Finally, the correction to the oblateness due to Ceres' polar aspect angle lies within the 1σ error bar and has no statistical relevance; hence $\epsilon = 0.08 \pm 0.03$.

2.4.2 Pole-constrained solution

At the occultation, the coordinates (equation 3) of Ceres' rotational pole correspond to the position angle $P = (12 \pm 3)^\circ$. Exploration of the parameter space, restricted to ellipses with position angles laying within this range, results in the pole-constrained solution. The related physical parameters are displayed on the third column of Table 2 in boldface, while the best-fitting solution is depicted in Fig. 3.

We notice that the constraint corresponds to the upper limit of nominal solution's 1σ error bar for P . On the other hand, it selects the smallest values of semimajor axis, improving its determination by a factor of about 2. Notwithstanding, oblateness' figures remain the same.

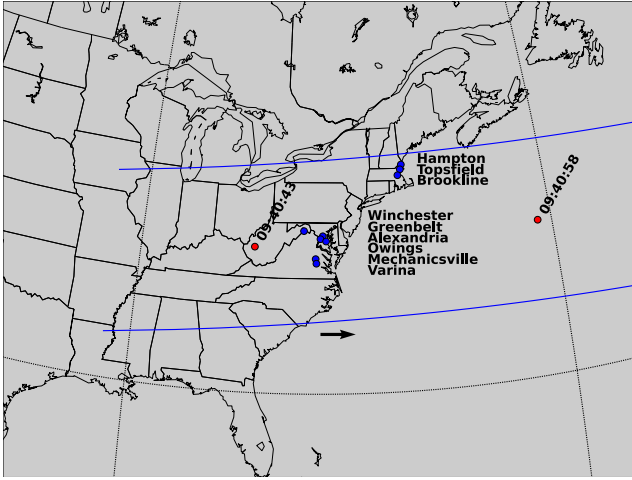


Figure 4. Post-occultation reconstruction of Ceres' shadow path on Earth for the 2013 October 25 event at the east coast of USA. Upper view of the occultation over the sites that observed the event (blue dots). Red points are the centre of the shadow separated by 15 s.

3 THE 2013 OCCULTATION

3.1 Observations

The event which took place on 2013 October 25 involved the star TYC 865-911-1 (UCAC4 496-058191), of magnitude $V = 10.05$.

Based on UCAC4 (Zacharias et al. 2013), the ICRS position to the date of occultation is

$$\begin{cases} \alpha = 11^{\text{h}}57^{\text{m}}52^{\text{s}}.7641 \\ \delta = +09^{\circ}07'49''.835. \end{cases} \quad (4)$$

The occultation could only be visible in the United States, before dawn, as depicted in Fig. 4.

Nine positive chords were obtained by the variety of instruments listed in Table 3. Each station was equipped with a video camera with negligible readout times. This was of particular importance, since in this event Ceres' shadow speed was 42.6 km s^{-1} , much faster than in the 2010 event.

Three different timing synchronization procedures were adopted among the set of observing stations. At Greenbelt and Owings, the 1PPS signal of a GPS unit was used to calibrate time stamps which were inserted at each frame of the video. Time extraction is thus straightforward, after taking camera delays into account. On the other hand, at Brookline the clock would be synchronized by an internet server. A lack of connection, however, resulted in spurious times. In fact, comparison between the times obtained at this station and the others suggests that the former have a delay of about 64 s. Therefore, we do not use Brookline's times in the analysis that follows. Finally, at the remaining six stations the videos were recorded by camcorders on digital tapes. The timing method consisted in the comparison of the camcorder internal clock to a 1PPS GPS signal, before and after the recording of the occultation. Absolute timing errors of this procedure are expected to be less than 0.1 s.

Table 3. Circumstances of observation for the observing stations of the 2013 event.

Site	Longitude Latitude Height	Telescope: Aperture f-ratio	Camera Cycle time	Result Ingress Egress	Observer
Hampton	70°48'59".7 W 42°53'52".8 N 7 m	12 cm f/5	PC164C-EX2 0.033 s	Positive 09:40:46.9 ± 0.1 s 09:40:57.26 ± 0.08 s	T. Blank
Topsfield	70°55'16".6 W 42°37'55".9 N 45 m	12 cm f/5	PC164C-EX2 0.033 s	Positive 09:40:45.4 ± 0.1 s 09:40:58.0 ± 0.1 s	T. Blank
Brookline	71°08'14".5 W 42°18'27".4 N 109 m	64 cm f/9.6	Infinity2-1R 0.015 s	Positive 09:41:48.00 ± 0.01 s 09:42:02.93 ± 0.01 s	N. Weber R. Dantowitz
Winchester	78°14'39".6 W 39°16'21".5 N 211 m	36 cm f/5	PC164C 0.033 s	Positive 09:40:33.26 ± 0.08 s 09:40:55.86 ± 0.09 s	J. Brooks
Greenbelt	76°52'09".4 W 38°59'12".1 N 52 m	12 cm f/2.5	PC164C-EX2 0.033 s	Positive 09:40:33.6 ± 0.1 s 09:40:56.4 ± 0.1 s	J. Dunham D. Dunham
Alexandria	77°02'28".3 W 38°49'19".1 N 8 m	7 cm f/10	Watec120N 0.067 s	Positive 09:40:33.3 ± 0.1 s 09:40:56.1 ± 0.1 s	P. Maley
Owings	76°38'06".3 W 38°41'26".5 N 38 m	25 cm f/3.3	PC164C 0.033 s	Positive 09:40:34.27 ± 0.05 s 09:40:56.0 ± 0.2 s	C. Ellington
Mechanicsville	77°23'06".7 W 37°41'26".1 N 60 m	12 cm f/2.5	PC164C-EX2 0.033 s	Positive 09:40:33.0 ± 0.1 s 09:40:54.8 ± 0.1 s	D. Dunham
Varina	77°19'49".3 W 37°25'58".6 N 19 m	12 cm f/2.5	PC164C-EX2 0.033 s	Positive 09:40:32.4 ± 0.3 s 09:40:53.1 ± 0.2 s	D. Dunham

During the event Ceres was low in the horizon, with altitudes between 15° (Winchester) and 20° (Hampton). Strong scintillation is expected in such a scenario which, combined to short integration times and the low magnitude drop of the event, resulted in rather noisy light curves and thus larger uncertainties in the time of the contacts, as is shown in the next section.

3.2 Light curves

All videos were converted to FITS images and the photometry of the target was obtained via PRAIA (Assafin et al. 2011). The light curves were normalized to the flux of a reference star when available on the field.

To reduce the noise, the data were binned by groups of five images – with the exception of Greenbelt, which was averaged in sets of 10. This procedure enlarges the effective integration times reported in Table 3 by a factor of 5 (or 10). As in the 2010 event, an additional normalization by a polynomial curve was applied.

The ingress and egress instants of the occultation were obtained by the same procedure explained in Section 2.2. Since the typical effective integration time used (0.17 s) translates to about 7 km in the celestial plane, and the Fresnel scale and star diameter are again of the order of a few hundreds of metres, the theoretical occultation light curves are largely dominated by the integration times, as for the 2010 event.

The best-fittings to the occultation light curves are shown in Fig. 5, and the derived occultation times are listed in Table 3.

3.3 Limb-fitting solutions

Elliptical limb profiles were adjusted to all the available³ chords by the same procedure described in Section 2.3. This yielded $\chi^2_{r,\min} = 13$, suggesting that an elliptical model is not satisfactory to the data. Indeed, a quick glance at a plot of the observed chords, such as in Fig. 6, shows that the Varina chord seems to be somewhat advanced with respect to the others. Taking into account that in this station time stamps were not inserted on the video frames, it is fairly possible to attribute this advance to an eventual problem on the correspondence between camcorder's and GPS' times. This could be caused, for example, if the camcorder delayed to start the recording and, since this was an unattended pre-pointed station, this fact would not be noticed by the analysis of the video itself.

The immersion recorded at Owings also seems to be shifted (delayed) with respect to the nearby chords (see Fig. 6). This chord, actually, has roughly the same length of Mechanicsville's, despite the fact that they are separated by about 100 km. Differently from Varina, though, this station had time stamps inserted in each frame of the video, which makes it more unlikely to justify an eventual timing issue. Another possible explanation for the apparent problem of the times of this chord is the determination of the ingress and egress instants in the light-curve analysis, which could have been affected by noise. Finally, the delay during the ingress could be caused by a relief feature in Ceres; we shall soon return to this hypothesis.

In a second limb fitting, thus, we did not consider Brookline, Varina, and Owings chords. The adjustment of the five parameters which define an ellipse to the 12 contacts then resulted in $\chi^2_{r,\min} = 1.27$, indicating that the fitting is in good agreement with

³ Brookline's chord was not used for limb fitting since it had an inaccurate absolute time.

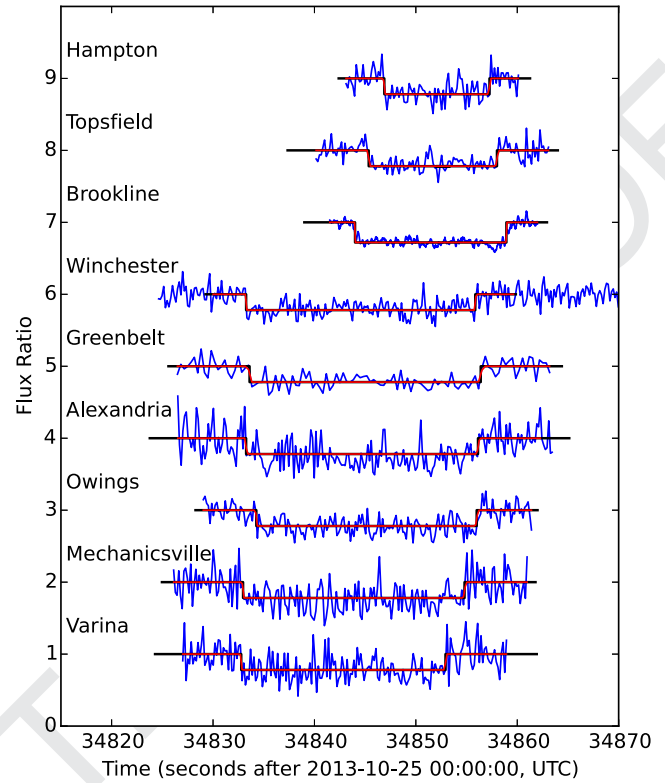


Figure 5. The nine occultation light curves normalized and vertically shifted by a factor of 1.0 for better viewing, see Fig. 2 for the explanation of the graph. The light curve of Brookline is shifted by -64 s as explained in the text.

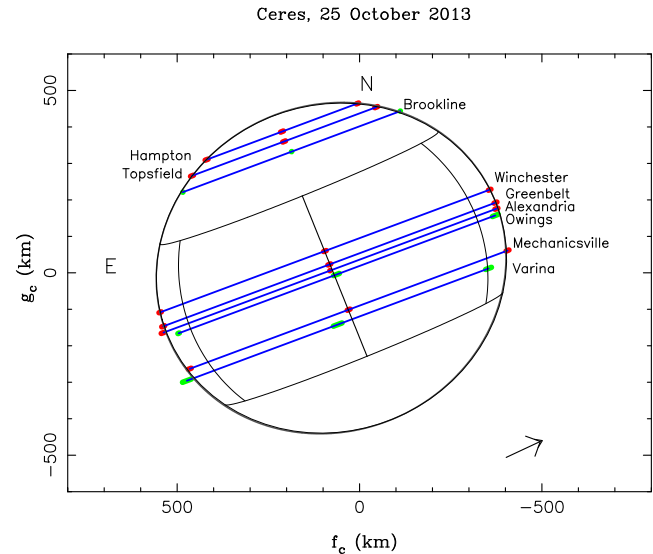


Figure 6. The best elliptical fit for the occultation chords for the event of 2013 using timing from Table 3 and the pole-constrained solution. The arrow indicates the direction of motion, blue lines are the observed chords, the red and green segments are the ingress, egress and mid-occultation error bars at 1σ level. The chords with green error bars were not used during the limb-fitting process. The chord of Brookline if shifted by -64 s as explained in the text.

the observed data within the error bars. This is the solution depicted in Fig. 6, where we see that the chord length measured in Brookline is compatible to the model. The associated physical parameters are presented in Table 2 as the nominal solution.

For this event the polar aspect angle is $\zeta = 90^\circ.7$, which makes the true oblateness equal to the apparent one, within the error bars.

The position angle of this nominal solution is better constrained than the 2010 occultation. Actually, the uncertainty in the former is of 5° in contrast to 10° of the latter. This suggests that the pole-constrained solution obtained via the position of Ceres' pole (equation 3) would not be significantly different from the nominal one.

This assumption was confirmed when we carried out the limb fitting with the constraint $P = (25 \pm 3)^\circ$, the position angle at the occultation which follows from equation (3). The physical parameters related to this pole-constrained solution are presented in the last column of Table 2, and are essentially the same of the nominal solution.

In the hypothesis that the delay observed in the immersion at Owings could be associated with a limb topography feature, the recorded contact would then correspond to a negative elevation of 31 ± 4 km with respect to the best-fitting ellipse. Theoretical models, however, predict that reliefs in Ceres should not be higher than about 10–20 km (Johnson & McGetchin 1973), while published observational data sets the bound of 18 km (Carry et al. 2008). More recently, images by the probe *Dawn* also reveal an even smoother surface. Therefore, the association of Owings first contact to a relief is improbable.

4 ASTROMETRY FROM OCCULTATIONS

The objects' geocentric positions derived from stellar occultations are most valuable for improving their orbits (Desmars et al. 2015). Usually the precision of the astrometric positions are limited by the accuracy of the occulted star position, not by the limb fit, Ceres' geocentric J2000 positions at the time of each occultation are displayed in equations (5) and (6). The errors of the positions come from the errors of the star positions, taken from the catalogues and from the errors of the relative apparent distances between star and Ceres, derived from the limb fit (which are displayed as $\Delta\alpha \cos \delta$, $\Delta\delta$),

$$2010 \text{ Aug } 17 \begin{cases} \text{Time} = 22 : 40 : 00 \\ \alpha = 17^{\text{h}}18^{\text{m}}29^{\text{s}}.0122 \pm 0''.027 \\ \delta = -27^\circ26'38''.617 \pm 0''.028 \\ \Delta\alpha \cos \delta = 0''.003; \Delta\delta = 0''.007 \end{cases} \quad (5)$$

$$2013 \text{ Oct } 25 \begin{cases} \text{Time} = 09 : 45 : 00 \\ \alpha = 11^{\text{h}}57^{\text{m}}52^{\text{s}}.9154 \pm 0''.019 \\ \delta = +09^\circ07'49''.865 \pm 0''.021 \\ \Delta\alpha \cos \delta = 0''.002; \Delta\delta = 0''.007. \end{cases} \quad (6)$$

5 DISCUSSION

A quick glance at Table 2 shows overall agreement between the physical parameters derived from both occultations, especially in the equatorial diameter. The differences of the solutions occur basically on the size of their error bars, and can be justified by the particularities of each set of data, as discussed below.

The 2010 event, for example, had only seven contacts; none the less, they were well distributed over Ceres' disc (see Fig. 3) acting as

Table 4. Ceres' equatorial diameter and oblateness.

Eq. diameter (km)	Oblateness	Method	Ref.
972 ± 6	0.08 ± 0.03	Occultation	1
967 ± 10	0.078 ± 0.015	Keck+VTL	2
959 ± 5	0.074 ± 0.007	Keck	3
975 ± 4	0.067 ± 0.005	<i>HST</i>	4
959 ± 5	0.05 ± 0.01	Occultation	5

References. 1: Present work. 2: Drummond et al. (2014). 3: Carry et al. (2008). 4: Thomas et al. (2005). 5: Millis et al. (1987).

a constraint to its shape. On the other hand, the 2013 event had five more exploitable contacts, but they were concentrated in certain regions of the body. In particular, the absence of chords close to Ceres' south pole made its oblateness less well determined here than in the 2010 event.

However, even our best measurement for the oblateness, $\epsilon = 0.08 \pm 0.03$, has still a higher uncertainty with regard to other figures published in the literature, as Table 4 shows. A larger number of uniformly spaced chords would be necessary to offer a best constraint to the oblateness.

The few chords of the 2010 occultation could themselves only constrain the position angle of the object to a uncertainty of 10° . This uncertainty was reduced by a factor of 2 in the 2013 event, approaching – and verifying – the result predicted by the work of Drummond et al. (2014). As was shown, using the coordinates of Ceres' polar axis to limit the position angle was not an efficient procedure in the 2013 event, in the sense that it did not result in significant changes in the parameters obtained in the nominal solution (see Table 2).

On the other hand, constraining the position angle on the 2010 occultation was proved to reduce the error bars of the other parameters (disregarding oblateness). Moreover, this procedure resulted in excellent agreement between the equatorial radius figures of both events.

The 2013 occultation, therefore, offers not only an independent verification of the figures resulted from the 2010 event, but also validates the procedure carried out there which led to the best-constrained parameters in this work.

Comparison of Ceres' equatorial diameter as measured by different techniques is carried out in Table 4. We note overall agreement between our result to those obtained via direct imaging by the *Hubble Space Telescope* (*HST*; Thomas et al. 2005), the Keck Observatory and the ESO VLT (Drummond et al. 2014). The smaller figure reported by Carry et al. (2008) may be justified by the fact that in this study the effects of limb darkening were not taken into account, as pointed out by Drummond et al. (2014).

As mentioned in the Introduction, the 1984 event (Millis et al. 1987) is the only occultation data to which we can compare our result. The measured diameters do not agree, ours being larger by 2σ . It is difficult to state for sure the reasons for this divergence. One way to clarify the issue is to redetermine the immersion and emersion instants from the original light curves using the same methodology presented in our work. Note that in this occultation a variation of 0.5 s in the contact times correspond to almost 7 km on Ceres' limb, which is on the same order of the residuals of their elliptical fit. However, we could not do that, as we had no access to the original 1984 light-curve data. Moreover, we have no description of how the immersion and emersion instants of the

chords were actually determined from these light curves in Millis et al. (1987).

NASA's *Dawn* mission shall bring light to these questions, which will be important not only for the knowledge of Ceres itself, but also for all the techniques used so far to study the physical properties of small Solar system objects, such as the stellar occultations.

ACKNOWLEDGEMENTS

ARGJ thanks the financial support of CAPES. BLG thanks CNPq. FBR acknowledges PAPDRJ-FAPERJ/CAPES E-43/2013 number 144997, E-26/101.375/2014, and CDFB-CAPES/Brazil. MA acknowledges CNPq grants 473002/2013-2, 482080/2009-4, and 312394/2014-4, and FAPERJ grant 111.488/2013. RVM thanks grants CNPq-306885/2013, Capes/Cofecub-2506/2015, and Faperj/PAPDRJ-45/2013. JIBC acknowledges CNPq for a PQ2 fellowship (process number 308489/2013-6). We also acknowledge Steve Preston for the predictions of the occultations and the referee Lawrence H. Wasserman (Lowell Observatory) for his contributions to improve the text.

REFERENCES

Assafin M. et al., 2011, in Tanga P., Thuillot W., eds, Gaia FUN-SSO Workshop Proc.: Gaia Follow-up Network for the Solar System Objects. IMCCE-Paris Observatory, Paris, p. 85

- Braga-Ribas F. et al., 2013, *ApJ*, 773, 26 (BR13)
- Braga-Ribas F. et al., 2014, *Nature*, 508, 72
- Carry B., Dumas C., Fulchignoni M., Merline W. J., Berthier J., Hestroffer D., Fusco T., Tamblyn P., 2008, *A&A*, 478, 235
- Castillo-Rogez J. C., 2011, *Icarus*, 215, 599
- Desmars J. et al., 2015, *A&A*, submitted
- Drummond J. D. et al., 2014, *Icarus*, 236, 28
- Dunham D. W., Herald D., Frappa E., Hayamizu T., Talbot J., Timerson B., 2014, Asteroid Occultations V12.0. NASA Planetary Data System, EAR-A-3-RDR-OCCULTATIONS-V12.0
- Giorgini J. D. et al., 1996, *BAAS*, 28, 1158
- Gomes R., Levison H. F., Tsiganis K., Morbidelli A., 2005, *Nature*, 435, 466
- Johnson T. V., McGetchin T. R., 1973, *Icarus*, 18, 612
- Küppers M. et al., 2014, *Nature*, 505, 525
- McKinnon W. B., 2012, *LPI Contrib.*, 1667, 6475
- Millis R. L. et al., 1987, *Icarus*, 72, 507
- Russell C. T. et al., 2004, *Planet. Space Sci.*, 52, 465
- Sicardy B. et al., 2011, *Nature*, 478, 493
- Thomas P. C., Parker J. W., McFadden L. A., Russell C. T., Stern S. A., Sykes M. V., Young E. F., 2005, *Nature*, 437, 224
- Widemann T. et al., 2009, *Icarus*, 199, 458
- Zacharias N., Finch C. T., Girard T. M., Henden A., Bartlett J. L., Monet D. G., Zacharias M. I., 2013, *AJ*, 145, 44

This paper has been typeset from a \LaTeX file prepared by the author.

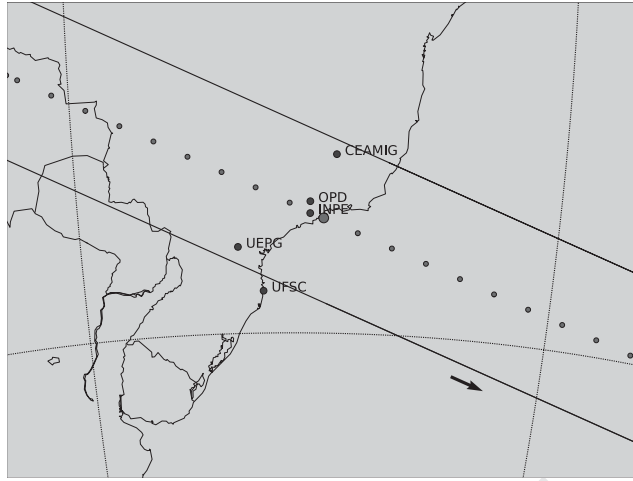


Figure 1. Post-occultation reconstruction of Ceres' shadow path on Earth for the 2010 August 17 event. The big red dot is the geocentric closest approach at 22:40:25 UT. The small red ones represent the centre of the shadow separated by one minute, shadow moves from the left to the right. Blue dots are the sites that have observed the event. As described in text, UFSC had a negative chord.

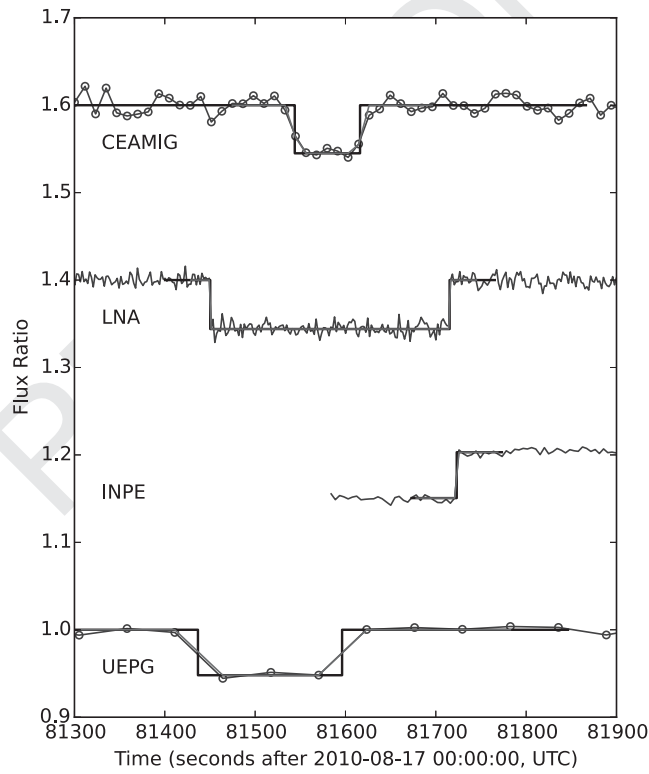


Figure 2. The four occultation light curves normalized and vertically shifted by a factor of 0.2 for better visualization. The solid black lines are the best fit of the square-well model to the data. Red lines are the square-well model convoluted with the Fresnel diffraction, the star diameter, and the applied exposure time. The mid-times of the occultations do not coincide due to the propagation delays of the shadow due to the distinct longitude of the sites. Exposures at INPE started after the immersion, as explained in the text.

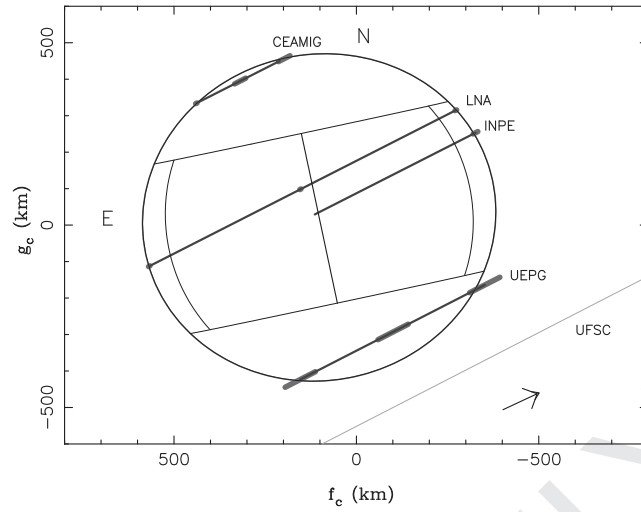


Figure 3. The best elliptical fit for the occultation chords for the event of 2010 using the times from Table 1 and the pole-constrained solution. The arrow indicates the direction of motion, blue lines are the observed chords, the red segments are the ingress, egress and mid-occultation error bars at 1σ level.

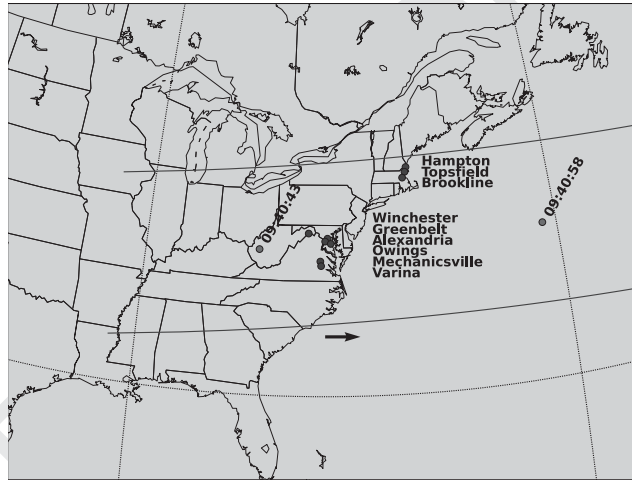


Figure 4. Post-occultation reconstruction of Ceres' shadow path on Earth for the 2013 October 25 event at the east coast of USA. Upper view of the occultation over the sites that observed the event (blue dots). Red points are the centre of the shadow separated by 15 s.

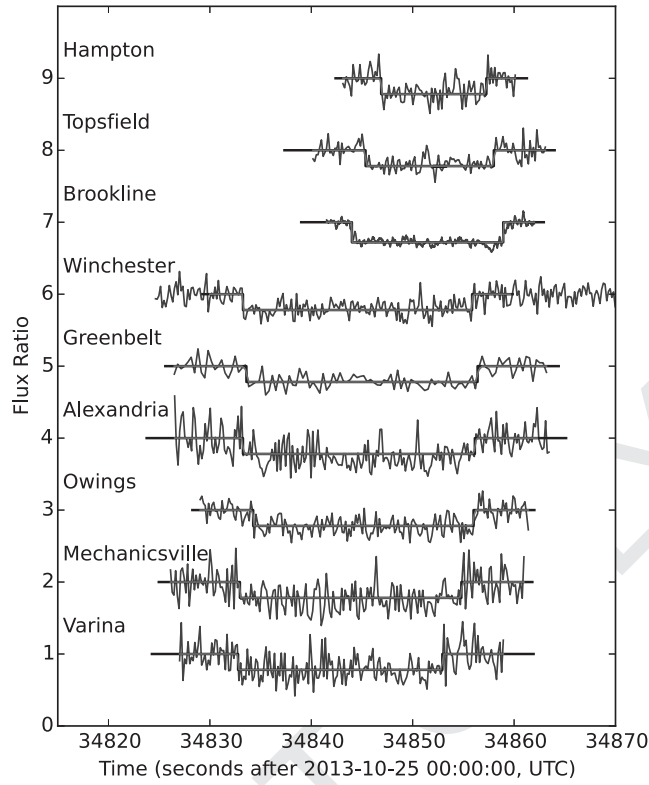


Figure 5. The nine occultation light curves normalized and vertically shifted by a factor of 1.0 for better viewing, see Fig. 2 for the explanation of the graph. The light curve of Brookline is shifted by -64 s as explained in the text.

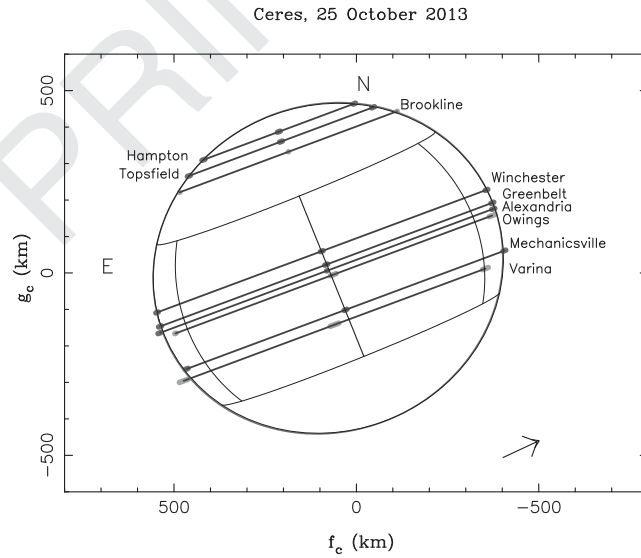


Figure 6. The best elliptical fit for the occultation chords for the event of 2013 using timing from Table 3 and the pole-constrained solution. The arrow indicates the direction of motion, blue lines are the observed chords, the red and green segments are the ingress, egress and mid-occultation error bars at 1σ level. The chords with green error bars were not used during the limb-fitting process. The chord of Brookline is shifted by -64 s as explained in the text.

List of astronomical key words

(updated 2013 July)

This list is common to *Monthly Notices of the Royal Astronomical Society*, *Astronomy and Astrophysics*, and *The Astrophysical Journal*. In order to ease the search, the key words are subdivided into broad categories. No more than *six* subcategories altogether should be listed for a paper.

The subcategories in boldface containing the word ‘individual’ are intended for use with specific astronomical objects; these should never be used alone, but always in combination with the most common names for the astronomical objects in question. Note that each object counts as one subcategory within the allowed limit of six.

The parts of the key words in italics are for reference only and should be omitted when the key words are entered on the manuscript.

General

editorials, notices
errata, addenda
extraterrestrial intelligence
history and philosophy of astronomy
miscellaneous
obituaries, biographies
publications, bibliography
sociology of astronomy
standards

Physical data and processes

acceleration of particles
accretion, accretion discs
asteroseismology
astrobiology
astrochemistry
astroparticle physics
atomic data
atomic processes
black hole physics
chaos
conduction
convection
dense matter
diffusion
dynamo
elementary particles
equation of state
gravitation
gravitational lensing: strong
gravitational lensing: weak
gravitational lensing: micro
gravitational waves
hydrodynamics
instabilities
line: formation
line: identification
line: profiles
magnetic fields

magnetic reconnection
(magnetohydrodynamics) MHD
masers
molecular data
molecular processes
neutrinos
nuclear reactions, nucleosynthesis, abundances
opacity
plasmas
polarization
radiation: dynamics
radiation mechanisms: general
radiation mechanisms: non-thermal
radiation mechanisms: thermal
radiative transfer
relativistic processes
scattering
shock waves
solid state: refractory
solid state: volatile
turbulence
waves

Astronomical instrumentation, methods and techniques

atmospheric effects
balloons
instrumentation: adaptive optics
instrumentation: detectors
instrumentation: high angular resolution
instrumentation: interferometers
instrumentation: miscellaneous
instrumentation: photometers
instrumentation: polarimeters
instrumentation: spectrographs
light pollution
methods: analytical
methods: data analysis
methods: laboratory: atomic
methods: laboratory: molecular
methods: laboratory: solid state
methods: miscellaneous
methods: numerical
methods: observational
methods: statistical
site testing
space vehicles
space vehicles: instruments
techniques: high angular resolution
techniques: image processing
techniques: imaging spectroscopy
techniques: interferometric
techniques: miscellaneous
techniques: photometric
techniques: polarimetric
techniques: radar astronomy
techniques: radial velocities

techniques: spectroscopic
telescopes

Astronomical data bases

astronomical data bases: miscellaneous
atlases
catalogues
surveys
virtual observatory tools

Astrometry and celestial mechanics

astrometry
celestial mechanics
eclipses
ephemerides
occultations
parallaxes
proper motions
reference systems
time

The Sun

Sun: abundances
Sun: activity
Sun: atmosphere
Sun: chromosphere
Sun: corona
Sun: coronal mass ejections (CMEs)
Sun: evolution
Sun: faculae, plages
Sun: filaments, prominences
Sun: flares
Sun: fundamental parameters
Sun: general
Sun: granulation
Sun: helioseismology
Sun: heliosphere
Sun: infrared
Sun: interior
Sun: magnetic fields
Sun: oscillations
Sun: particle emission
Sun: photosphere
Sun: radio radiation
Sun: rotation
(*Sun*.) solar–terrestrial relations
(*Sun*.) solar wind
(*Sun*.) sunspots
Sun: transition region
Sun: UV radiation
Sun: X-rays, gamma-rays

Planetary systems

comets: general
comets: individual: ...
Earth
interplanetary medium
Kuiper belt: general
Kuiper belt objects: individual: ...

meteorites, meteors, meteoroids
minor planets, asteroids: general
minor planets, asteroids: individual: ...
Moon

Oort Cloud
planets and satellites: atmospheres
planets and satellites: aurorae
planets and satellites: composition
planets and satellites: detection
planets and satellites: dynamical evolution and stability
planets and satellites: formation
planets and satellites: fundamental parameters
planets and satellites: gaseous planets
planets and satellites: general
planets and satellites: individual: ...
planets and satellites: interiors
planets and satellites: magnetic fields
planets and satellites: oceans
planets and satellites: physical evolution
planets and satellites: rings
planets and satellites: surfaces
planets and satellites: tectonics
planets and satellites: terrestrial planets
planet–disc interactions`
planet–star interactions
protoplanetary discs
zodiacal dust

Stars

stars: abundances
stars: activity
stars: AGB and post-AGB
stars: atmospheres
(*stars*.) binaries (*including multiple*): close
(*stars*.) binaries: eclipsing
(*stars*.) binaries: general
(*stars*.) binaries: spectroscopic
(*stars*.) binaries: symbiotic
(*stars*.) binaries: visual
stars: black holes
(*stars*.) blue stragglers
(*stars*.) brown dwarfs
stars: carbon
stars: chemically peculiar
stars: chromospheres
(*stars*.) circumstellar matter
stars: coronae
stars: distances
stars: dwarf novae
stars: early-type
stars: emission-line, Be
stars: evolution
stars: flare
stars: formation
stars: fundamental parameters
(*stars*.) gamma-ray burst: general
(*stars*.) **gamma-ray burst: individual: ...**
stars: general
(*stars*.) Hertzsprung–Russell and colour–magnitude diagrams
stars: horizontal branch
stars: imaging
stars: individual: ...

- stars: interiors
- stars: jets
- stars: kinematics and dynamics
- stars: late-type
- stars: low-mass
- stars: luminosity function, mass function
- stars: magnetars
- stars: magnetic field
- stars: massive
- stars: mass-loss
- stars: neutron
- (stars:) novae, cataclysmic variables
- stars: oscillations (*including pulsations*)
- stars: peculiar (*except chemically peculiar*)
- (stars:) planetary systems
- stars: Population II
- stars: Population III
- stars: pre-main-sequence
- stars: protostars
- (stars:) pulsars: general
- (stars:) **pulsars: individual: ...**
- stars: rotation
- stars: solar-type
- (stars:) starspots
- stars: statistics
- (stars:) subdwarfs
- (stars:) supergiants
- (stars:) supernovae: general
- (stars:) **supernovae: individual: ...**
- stars: variables: Cepheids
- stars: variables: δ Scuti
- stars: variables: general
- stars: variables: RR Lyrae
- stars: variables: S Doradus
- stars: variables: T Tauri, Herbig Ae/Be
- (stars:) white dwarfs
- stars: winds, outflows
- stars: Wolf–Rayet

Interstellar medium (ISM), nebulae

- ISM: abundances
- ISM: atoms
- ISM: bubbles
- ISM: clouds
- (ISM:) cosmic rays
- (ISM:) dust, extinction
- ISM: evolution
- ISM: general
- (ISM:) H II regions
- (ISM:) Herbig–Haro objects
- ISM: individual objects: ...**
- (*except planetary nebulae*)
- ISM: jets and outflows
- ISM: kinematics and dynamics
- ISM: lines and bands
- ISM: magnetic fields
- ISM: molecules
- (ISM:) planetary nebulae: general
- (ISM:) **planetary nebulae: individual: ...**
- (ISM:) photodissociation region (PDR)
- ISM: structure
- ISM: supernova remnants

The Galaxy

- Galaxy: abundances
- Galaxy: bulge
- Galaxy: centre
- Galaxy: disc
- Galaxy: evolution
- Galaxy: formation
- Galaxy: fundamental parameters
- Galaxy: general
- (Galaxy:) globular clusters: general
- (Galaxy:) **globular clusters: individual: ...**
- Galaxy: halo
- Galaxy: kinematics and dynamics
- (Galaxy:) local interstellar matter
- Galaxy: nucleus
- (Galaxy:) open clusters and associations: general
- (Galaxy:) **open clusters and associations: individual: ...**
- (Galaxy:) solar neighbourhood
- Galaxy: stellar content
- Galaxy: structure

Galaxies

- galaxies: abundances
- galaxies: active
- (galaxies:) BL Lacertae objects: general
- (galaxies:) **BL Lacertae objects: individual: ...**
- galaxies: bulges
- galaxies: clusters: general
- galaxies: clusters: individual: ...**
- galaxies: clusters: intracluster medium
- galaxies: distances and redshifts
- galaxies: dwarf
- galaxies: elliptical and lenticular, cD
- galaxies: evolution
- galaxies: formation
- galaxies: fundamental parameters
- galaxies: general
- galaxies: groups: general
- galaxies: groups: individual: ...**
- galaxies: haloes
- galaxies: high-redshift
- galaxies: individual: ...**
- galaxies: interactions
- (galaxies:) intergalactic medium
- galaxies: irregular
- galaxies: ISM
- galaxies: jets
- galaxies: kinematics and dynamics
- (galaxies:) Local Group
- galaxies: luminosity function, mass function
- (galaxies:) Magellanic Clouds
- galaxies: magnetic fields
- galaxies: nuclei
- galaxies: peculiar
- galaxies: photometry
- (galaxies:) quasars: absorption lines
- (galaxies:) quasars: emission lines
- (galaxies:) quasars: general
- (galaxies:) **quasars: individual: ...**
- (galaxies:) quasars: supermassive black holes
- galaxies: Seyfert

galaxies: spiral
galaxies: starburst
galaxies: star clusters: general
galaxies: star clusters: individual: ...
galaxies: star formation
galaxies: statistics
galaxies: stellar content
galaxies: structure

Cosmology

(*cosmology:*) cosmic background radiation
(*cosmology:*) cosmological parameters
cosmology: miscellaneous
cosmology: observations
cosmology: theory
(*cosmology:*) dark ages, reionization, first stars
(*cosmology:*) dark energy
(*cosmology:*) dark matter
(*cosmology:*) diffuse radiation
(*cosmology:*) distance scale
(*cosmology:*) early Universe
(*cosmology:*) inflation
(*cosmology:*) large-scale structure of Universe
(*cosmology:*) primordial nucleosynthesis

Resolved and unresolved sources as a function of wavelength

gamma-rays: diffuse background
gamma-rays: galaxies
gamma-rays: galaxies: clusters
gamma-rays: general
gamma-rays: ISM
gamma-rays: stars
infrared: diffuse background

infrared: galaxies
infrared: general
infrared: ISM
infrared: planetary systems
infrared: stars
radio continuum: galaxies
radio continuum: general
radio continuum: ISM
radio continuum: planetary systems
radio continuum: stars
radio lines: galaxies
radio lines: general
radio lines: ISM
radio lines: planetary systems
radio lines: stars
submillimetre: diffuse background
submillimetre: galaxies
submillimetre: general
submillimetre: ISM
submillimetre: planetary systems
submillimetre: stars
ultraviolet: galaxies
ultraviolet: general
ultraviolet: ISM
ultraviolet: planetary systems
ultraviolet: stars
X-rays: binaries
X-rays: bursts
X-rays: diffuse background
X-rays: galaxies
X-rays: galaxies: clusters
X-rays: general
X-rays: individual: ...
X-rays: ISM
X-rays: stars